Geometry, Imaging and Computing
Volume 1, Number 2, 223–258, 2014

High performance computing for spherical conformal and Riemann mappings

Wei-Qiang Huang, Xianfeng David Gu, Tsung-Ming Huang, Song-Sun Lin, Wen-Wei Lin, and Shing-Tung Yau

A classical way of finding the harmonic map is to minimize the harmonic energy by the time evolution of the solution of a nonlinear heat diffusion equation. To arrive at the desired harmonic map, which is a steady-state of this equation, we propose an efficient quasi-implicit Euler method and analyze its convergence under some simplifications. If the initial map is not close to the steady-state solution, it is difficult to find the stability region of the time steps. To remedy this drawback, we propose a two-phase approach for the quasi-implicit Euler method. In order to accelerate the convergence, a variant time step scheme and a heuristic method to determine an initial time step are developed. Numerical results clearly demonstrate that the proposed method achieves high performance for computing the spherical conformal and Riemann mappings.

Keywords and phrases: Spherical conformal mapping, Riemann mapping, nonlinear heat diffusion equation, quasi-implicit Euler method, adaptive controlling time step, two-phase.

1. Introduction

Conformal surface parameterizations have been studied intensively, and most works deal with genus zero surfaces. The basic approaches are harmonic energy minimization [1, 3, 5, 11, 21, 26], Cauchy-Riemann equation approximation [24], Laplacian operator linearization [2, 15], angle-based flattening method [28, 29] and circle packing [18, 19], among others. In harmonic energy minimization, a discrete harmonic map is introduced in [5] to approximate the continuous harmonic map by minimizing a metric dispersion criterion. Due to the conformal nature of harmonic maps from a genus zero closed surfaces to the unit sphere, Gu and Yau [11] proposed a nonlinear optimization method by minimizing the harmonic energy iteratively on the unit sphere until convergence to a harmonic map. The method has been ap-

plied to brain mapping [9, 32], surface classification [13] and global surface parameterizations [12].

The evolution of computing a conformal map $\mathbf{f}$ from genus zero closed surfaces to the unit sphere is carried out by a nonlinear heat diffusion equation

$$\frac{d\mathbf{f}}{dt} = -\Delta\mathbf{f}, \tag{1}$$

with $\mathbf{f}$ to be constrained on the unit sphere. In [9, 11, 14], the explicit (forward) Euler method has been used to produce a steady-state solution of the nonlinear heat diffusion equation (1). The explicit scheme is attractive for its simplicity. Unfortunately, it is known to have a small stability region that leads to extremely small time steps. While the implicit (backward) Euler method has a much larger stability region, it involves nonlinear systems. In this step, it is crucial to have a successful iterative method and a good way to produce the associated initial guess when the time step is relatively large. To tackle this challenging problem, the semi-implicit Euler methods [4, 8, 30, 31, 34] have been proposed to simplify the nonlinearity of the systems and improve the computational cost in each iteration. In this paper, we propose a two-phase approach for the underlying quasi-implicit Euler method (QIEM) to solve the nonlinear heat diffusion equation (1). Phase-I QIEM is used to quickly find an approximate solution which is close to the steady-state solution; Phase-II QIEM is then applied to compute the steady-state solution using the approximate solution produced by Phase-I QIEM. The advantages of the two-phase QIEM are that it only needs to solve a linear system and allows a large time step in each iteration.

For the iterative methods of solving the steady-state ODE systems, the adaptive methods [7, 16, 22, 34] for controlling the time step in each iteration are proposed to accelerate its convergence. In this paper, we not only propose a heuristic method to estimate the initial time step, but also develop an adaptive method to control the time step so that the two-phase QIEM possesses high performance. Promising numerical results illustrate the efficiency and stability of the proposed algorithms.

This paper is outlined as follows. In Section 2, we briefly discuss the conformal mappings for genus zero surfaces. In Section 3, the quasi-implicit Euler method is proposed to solve the nonlinear heat diffusion equation (1). Convergence of the simplified QIEM with suitable assumptions is shown in Section 4. In Section 5, we propose a practical two-phase QIEM. A heuristic method to estimate the initial time step and an adaptive method to control the time step are also proposed in this section. Numerical experiments

to validate and measure the timing performance of the proposed schemes are demonstrated in Section 6. Finally, we conclude the paper in the last section.

2. Conformal mappings

2.1. Spherical conformal mapping

In this subsection, we introduce the spherical conformal mapping for genus zero closed surfaces from the point of view that a map is conformal if and only if it is harmonic. That is, we shall introduce how to use the heat flow method to deform a mapping into the harmonic map under a special normalization condition.

Suppose M is a triangular mesh of a genus zero closed surface with n vertices $\{v_1, \cdots, v_n\}$. We denote all piecewise linear functions defined on M by $C^{PL}(M)$, which forms a linear space.

Definition 2.1 (Discrete harmonic energy)**.** *Let* $\mathbf{f} = (f_1, f_2, f_3) : M \to \mathbb{R}^3$ *with* $f_1, f_2, f_3 \in C^{PL}(M)$*. The harmonic energy of* $\mathbf{f}$ *is defined as*

$$\mathcal{E}_h(\mathbf{f}) = \sum_{\ell=1}^{3} \mathcal{E}_h(f_\ell) \tag{2a}$$

with

$$\mathcal{E}_h(f_\ell) = \frac{1}{2} \sum_{[v_i, v_j] \in M} k_{ij} \left(f_\ell(v_i) - f_\ell(v_j)\right)^2, \ \ell = 1, 2, 3, \tag{2b}$$

where $\{k_{ij}\}$ *forms a set of harmonic weights assigned on each edge* $[v_i, v_j] \in M$ *and is chosen such that the quadratic form of* (2b) *is positive definite.*

Definition 2.2. *Let* $\mathbf{f} = (f_1, f_2, f_3) : M \to \mathbb{R}^3$ *with* $f_1, f_2, f_3 \in C^{PL}(M)$*. The piecewise Laplacian operator of* $\mathbf{f}$ *is defined by*

$$\Delta_d \mathbf{f} = (\Delta_d f_1, \Delta_d f_2, \Delta_d f_3)$$

with

$$\Delta_d f_\ell(v_i) = \sum_{[v_i, v_j] \in M} k_{ij} \left(f_\ell(v_i) - f_\ell(v_j)\right), \ \ell = 1, 2, 3,$$

in which k_{ij} *are the harmonic weights in* (2b)*.*

Let $\mathbf{f}(v)$ and $\mathbf{n}(\mathbf{f}(v))$ denote the image of the vertex $v \in M$ and the normal on the target plane at $\mathbf{f}(v)$, respectively. Then the normal and tangent components of $\Delta_d \mathbf{f}$ are defined as

$$(\Delta_d \mathbf{f}(v))^{\perp} = < \Delta_d \mathbf{f}(v), \mathbf{n}(\mathbf{f}(v)) > \mathbf{n}(\mathbf{f}(v)) \tag{3}$$

and

$$(\Delta_d \mathbf{f}(v))^{\parallel} = \Delta_d \mathbf{f}(v) - (\Delta_d \mathbf{f}(v))^{\perp}, \tag{4}$$

respectively, where $< \cdot, \cdot >$ denotes the inner product in $\mathbb{R}^3$. Moreover, a map $\mathbf{f} : M_1 \to M_2$ is harmonic, if and only if $\mathbf{f}$ only has a normal component, and the tangential component is zero, i.e.,

$$\Delta_d \mathbf{f} = (\Delta_d \mathbf{f})^{\perp}. \tag{5}$$

Remark 2.1. *Note that if we take*

$$a_{ii} := \sum_{[v_i, v_j] \in M} k_{ij}, \quad a_{ij} := -k_{ij}, \ i \neq j, \tag{6}$$

for $i, j = 1, \ldots, n$ and define $A \equiv [a_{ij}] \in \mathbb{R}^{n \times n}$, then the discrete Laplacian operator $\Delta_d \mathbf{f}$ in (2) can be represented as the matrix form

$$\Delta_d \mathbf{f} = A\mathbf{f} = (Af_1, Af_2, Af_3).$$

Many different ways [1, 3, 5, 10, 11] are proposed to determine the edge weights k_{ij} in (2) so that the associated coefficient matrix A in (6) is symmetric positive semi-definite. A widely used edge weighting is the cotangent weighting proposed in [26]. The matrix A associated with cotangent weights has been shown to be symmetric positive semi-definite [17].

A classical way to find the harmonic map $\mathbf{f} : M \to \mathbb{S}^2$ is to minimize the discrete harmonic energy (2) by time evolution according to the nonlinear heat diffusion process

$$\frac{d\mathbf{f}}{dt} = -\Delta_d \mathbf{f}.$$

However, $\mathbf{f}(M, t)$ is constrained on the unit sphere $\mathbb{S}^2$ so that it needs to project $-\Delta_d \mathbf{f}$ onto the tangent plane of the sphere. Therefore, from (3)–(5), the evolution of $\mathbf{f}$ is according to the nonlinear heat diffusion equation:

$$\frac{d\mathbf{f}(v)}{dt} = -(\Delta_d \mathbf{f}(v))^{\parallel} = -(\Delta_d \mathbf{f}(v) - < \Delta_d \mathbf{f}(v), \mathbf{n}(\mathbf{f}(v)) > \mathbf{n}(\mathbf{f}(v))). \tag{7}$$

One major difficulty is that the solution to the conformal mapping from M to $\mathbb{S}^2$ is not unique but forms a Möbius group. In order to determine a unique solution, the additional zero mass-center constraint is required.

Definition 2.3. *A mapping* $\mathbf{f} : M_1 \to M_2$ *satisfies the zero mass-center condition if and only if*

$$\int_{M_1} \mathbf{f} d\sigma_{M_1} = 0,$$

where $d\sigma_{M_1}$ *is the area element on* M_1.

All conformal maps from M to $\mathbb{S}^2$ satisfying the zero mass-center constraint are unique up to the Euclidean rotation group.

2.2. Riemann mapping

The spherical conformal mapping for genus zero closed surfaces can be utilized to find a conformal mapping (Riemann mapping) from a simply connected surface M with a single boundary ∂M to a two-dimensional (2D) unit disk $\mathbb{D}$. The procedures for finding Riemann mapping are stated as follows. For a given simply connected triangular mesh M with boundary ∂M, there exists a symmetric closed surface M_c, called a double covering of M [10], which covers M twice, i.e., for each face in M, there are two preimages in M_c. Applying the spherical conformal mapping to M_c, a conformal map from M_c to the unit sphere $\mathbb{S}^2$ is found. Next, a Möbius transformation $\tau : \bar{\mathbb{C}} \to \bar{\mathbb{C}}$

$$\tau(z) = \frac{az + b}{cz + d}, \ a, b, c, d \in \mathbb{C}, \ ad - bc = 1$$

is used to adjust the conformal map such that ∂M is mapped to the equator of the unit sphere. Finally, the stereographic projection $\phi : \mathbb{S}^2 \to \mathbb{C}$

$$\phi(x, y, z) = \left(\frac{x}{1 - z}, \frac{y}{1 - z} \right), \ (x, y, z) \in \mathbb{S}^2$$

is applied to map the lower hemisphere conformally to the unit disk $\mathbb{D}$.

3. Quasi-implicit Euler method

Solving the steady-state problems in (7) is the most time consuming step in finding conformal mappings. In this section, we shall propose an efficient algorithm to solve (7).

For convenience, we give the following definition.

Definition 3.1. *Given*

$$\mathbf{u} \equiv \begin{bmatrix} \mathbf{u}_1 \\ \vdots \\ \mathbf{u}_n \end{bmatrix} \in \mathbb{R}^{n\times 3}, \quad \mathbf{v} \equiv \begin{bmatrix} \mathbf{v}_1 \\ \vdots \\ \mathbf{v}_n \end{bmatrix} \in \mathbb{R}^{n\times 3},$$

we define the operator $\prec \mathbf{u}, \mathbf{v} \succ$ *as*

$$\prec \mathbf{u}, \mathbf{v} \succ = diag\left(\mathbf{u}_1\mathbf{v}_1^\top, \cdots, \mathbf{u}_n\mathbf{v}_n^\top\right).$$

3.1. Explicit and implicit Euler methods

For solving the steady-state problem in (7), an explicit (forward) Euler method has been proposed in [9, 11, 14] by the following updating

$$\begin{aligned} \frac{\mathbf{f}^{(m+1)} - \mathbf{f}^{(m)}}{\delta t} &= -\left(\Delta_d \mathbf{f}^{(m)} - \prec \Delta_d \mathbf{f}^{(m)}, \mathbf{f}^{(m)} \succ \mathbf{f}^{(m)}\right) \\ &= -\left(A - \prec A\mathbf{f}^{(m)}, \mathbf{f}^{(m)} \succ\right) \mathbf{f}^{(m)}. \end{aligned}$$

Here the matrix A is the coefficient matrix of the Laplacian operator as in (6) with the edge weights k_{ij}. The advantage of the explicit Euler method is that it only needs matrix-vector multiplications in each iteration. By choosing time step δt carefully, the associated energy can be monotonically diminished at each iteration [9], for example, when δt is chosen close to the square of the minimum of the edge lengths of M [11]. However, in order to ensure numerical stability, the explicit technique always requires a very small time step which results in a significant drawback – a very slow convergence rate.

To remedy this obstacle, one may apply the implicit (backward) Euler method, which is A-stable over a wide range of time steps, to solve (7) as follows:

$$\begin{aligned} \frac{\mathbf{f}^{(m+1)} - \mathbf{f}^{(m)}}{\delta t} &= -\left(\Delta_d \mathbf{f}^{(m+1)} - \prec \Delta_d \mathbf{f}^{(m+1)}, \mathbf{f}^{(m+1)} \succ \mathbf{f}^{(m+1)}\right) \\ &= -\left(A - \prec A\mathbf{f}^{(m+1)}, \mathbf{f}^{(m+1)} \succ\right) \mathbf{f}^{(m+1)}, \end{aligned} \tag{8}$$

or equivalently,

$$\left[I + (\delta t)A\right] \mathbf{f}^{(m+1)} - (\delta t) \prec A\mathbf{f}^{(m+1)}, \mathbf{f}^{(m+1)} \succ \mathbf{f}^{(m+1)} = \mathbf{f}^{(m)}.$$

We may rewrite the above equation as the nonlinear systems $F(\mathbf{f}^{(m+1)}, \mathbf{f}^{(m)}) = 0$, where

$$F(\mathbf{f}^{(m+1)}, \mathbf{f}^{(m)}) \equiv -\text{vec}\left(\mathbf{f}^{(m)}\right) + \left\{(I_3 \otimes [I + (\delta t)A]) - (\delta t)\left(I_3 \otimes \prec A\mathbf{f}^{(m+1)}, \mathbf{f}^{(m+1)} \succ\right)\right\} \text{vec}\left(\mathbf{f}^{(m+1)}\right).$$

The unknown vectors $\mathbf{f}^{(m+1)}$ of $F(\mathbf{f}^{(m+1)}, \mathbf{f}^{(m)})$ can be solved by Newton's method

$$\text{vec}\left(\mathbf{f}_{i+1}^{(m+1)}\right) = \text{vec}\left(\mathbf{f}_{i}^{(m+1)}\right) - J\left(\mathbf{f}_{i}^{(m+1)}\right)^{-1} F(\mathbf{f}_{i}^{(m+1)}, \mathbf{f}^{(m)}) \tag{9}$$

with $\mathbf{f}_0^{(m+1)} = \mathbf{f}^{(m)}$, where $J(\mathbf{f}^{(m+1)})$ is the Jacobian matrix of $F(\mathbf{f}^{(m+1)}, \mathbf{f}^{(m)})$.

The implicit Euler method in (8) required to solve a linear system if Newton's method is applied. Although the Jacobian matrix $J(\mathbf{f}_i^{(m+1)})$ can be reordered as a banded matrix (see Appendix and Figure 9) so that direct methods can be applied, its size is enlarged to three times that of the matrix A.

3.2. Quasi-implicit Euler method

In order to avoid solving the nonlinear system in implicit Euler methods, some semi-implicit Euler methods [4, 8, 30, 31, 34] have been proposed to improve the computational cost in each iteration. Based on these, we propose the following quasi-implicit Euler method (QIEM) for solving the nonlinear heat diffusion equation in (7):

$$\begin{aligned}\frac{\mathbf{f}^{(m+1)} - \mathbf{f}^{(m)}}{\delta t} &= -\left(\Delta_d \mathbf{f}^{(m+1)} - \prec \Delta_d \mathbf{f}^{(m)}, \mathbf{f}^{(m)} \succ \mathbf{f}^{(m+1)}\right) \\ &= -\left(A - \prec A\mathbf{f}^{(m)}, \mathbf{f}^{(m)} \succ\right) \mathbf{f}^{(m+1)}.\end{aligned}$$

That is, in each iteration, the new vector $\mathbf{f}^{(m+1)}$ is generated by solving the linear system

$$\left[I + \delta t\left(A - \prec A\mathbf{f}^{(m)}, \mathbf{f}^{(m)} \succ\right)\right] \mathbf{f}^{(m+1)} = \mathbf{f}^{(m)}. \tag{10}$$

As an implicit Euler method, the QIEM has a wider range of stable time steps. Moreover, according to the discussion at the end of Subsection 3.1,

we see that QIEM is much more efficient than the implicit Euler method by comparing the computational costs of solving the linear systems in (9) and (10).

4. Convergence analysis of QIEM

In this section, we analyze the convergence of QIEM under the simplification of normalization of $\mathbf{f}^{(m+1)}$.

The QIEM with simplification of the normalization of $\mathbf{f}^{(m+1)}$ is stated as follows. Given $\mathbf{f}^{(0)} \in \mathbb{R}^{n\times 3}$ with $\|e_i^\top \mathbf{f}^{(0)}\|_2 = \frac{1}{\sqrt{n}}$ for $i = 1, \ldots, n$, i.e., $\|\mathbf{f}^{(0)}\|_F = 1$, we define $\mathbf{f}^{(m+1)}$ by

$$\mathbf{f}^{(m+1)} = \frac{1}{\sqrt{n}} D_m^{-1/2} A_m^{-1} \mathbf{f}^{(m)}, \tag{11}$$

for $m = 0, 1, \ldots$, where

$$A_m = I + \delta t \left(A- \prec A\mathbf{f}^{(m)}, \mathbf{f}^{(m)} \succ \right), \tag{12}$$

$$D_m = \prec A_m^{-1}\mathbf{f}^{(m)}, A_m^{-1}\mathbf{f}^{(m)} \succ . \tag{13}$$

Note that $\|e_i^\top \mathbf{f}^{(m+1)}\|_2 = \frac{1}{\sqrt{n}}$ for $i = 1, \ldots, n$ and $\|\mathbf{f}^{(m+1)}\|_F = 1$.

Let us consider the Schur decomposition

$$Q_m \Lambda_m Q_m^\top = A- \prec A\mathbf{f}^{(m)}, \mathbf{f}^{(m)} \succ,$$

where $Q_m \equiv [q_{1,m}, \cdots, q_{n,m}]^\top$ is orthonormal and $\Lambda_m = \mathrm{diag}(\lambda_1^{(m)}, \cdots, \lambda_n^{(m)})$ with $\lambda_i^{(m)}$ being the eigenvalues. Here, we assume $\lambda_i^{(m)} \neq 0$ for $i = 1, \ldots, n$. Then

$$\begin{aligned}
\frac{1}{\sqrt{n}} \|D_m^{-1/2}\|_2 &= \frac{1}{\sqrt{n}} \max_i \{\|e_i^\top A_m^{-1}\mathbf{f}^{(m)}\|_2^{-1}\} \\
&= \frac{1}{\sqrt{n}} \max_i \left\{ \|q_{i,m}^\top \left(I + \delta t \Lambda_m\right)^{-1} Q_m^\top \mathbf{f}^{(m)}\|_2^{-1} \right\} \\
&= \frac{\delta t}{\sqrt{n}} \max_i \left\{ \|q_{i,m}^\top \Lambda_m^{-1} Q_m^\top \mathbf{f}^{(m)} + \mathcal{O}_m\left(\frac{1}{\delta t}\right) \|_2^{-1} \right\}, \qquad (14)
\end{aligned}$$

where $\mathcal{O}_m\left(1/\delta t\right)$ is dependent on (i, m). Given a small positive value $\eta_m > 0$, there exists $T_0 > 0$ such that

$$\|\mathcal{O}_m\left(\frac{1}{\delta t}\right)\|_2 \leq \eta_m, \ \forall\ \delta t \geq T_0 \tag{15}$$

which implies that

$$\frac{1}{\sqrt{n}}\|D_m^{-1/2}\|_2 \le \frac{\delta t}{\sqrt{n}} \max_i \left\{ \left| \|q_i^\top \Lambda_m^{-1} Q_m^\top \mathbf{f}^{(m)}\|_2 - \eta_m \right|^{-1} \right\} \equiv \frac{\delta t}{\sqrt{n}} \frac{1}{a_m}. \tag{16}$$

By the definition of $\mathbf{f}^{(m+1)}$ in (11), it holds that

$$\begin{aligned} E_{m+1} &\equiv \mathbf{f}^{(m+1)} - \mathbf{f}^{(m)} \\ &= \frac{1}{\sqrt{n}} D_m^{-1/2} A_m^{-1} E_m + \frac{1}{\sqrt{n}} D_m^{-1/2} \left(A_m^{-1} - A_{m-1}^{-1} \right) \mathbf{f}^{(m-1)} \\ &\quad + \frac{1}{\sqrt{n}} \left(D_m^{-1/2} - D_{m-1}^{-1/2} \right) A_{m-1}^{-1} \mathbf{f}^{(m-1)}. \end{aligned} \tag{17}$$

Assume

$$|1 - \delta t \underline{\lambda}_m| = \min_i |1 + \delta t \lambda_i^{(m)}| > 1 \tag{18}$$

for $\delta t > 0$, where $\underline{\lambda}_m > 0$.

Lemma 4.1. *Let A_m, D_m and E_m be defined in (12), (13) and (17), respectively. Let a_m and $\underline{\lambda}_m$ be defined in (16) and (18), respectively. Assume*

$$\sqrt{n} a_m \underline{\lambda}_m - 3 > 0. \tag{19}$$

Then

$$\frac{1}{\sqrt{n}} \|D_m^{-1/2} A_m^{-1} E_m\|_F < \frac{1}{3} \|E_m\|_F$$

for all

$$\delta t > T_1 \equiv \max \left\{ \frac{\sqrt{n} a_m}{\sqrt{n} a_m \underline{\lambda}_m - 3}, T_0 \right\}$$

where T_0 is defined in (15).

Proof. From the assumption in (19), we have

$$\left(\sqrt{n} a_m \underline{\lambda}_m - 3 \right) \delta t > \sqrt{n} a_m, \quad \text{for } \delta t > T_1$$

which is equivalent to

$$-3\delta t > \sqrt{n} a_m \left(1 - \delta t \underline{\lambda}_m \right)$$

and then

$$3\delta t < \sqrt{n} a_m |1 - \delta t \underline{\lambda}_m|. \tag{20}$$

Combing the results in (16) and (20), it holds that

$$\frac{1}{\sqrt{n}} \|D_m^{-1/2} A_m^{-1} E_m\|_F \leq \frac{1}{\sqrt{n}} \frac{\delta t}{a_m |1 - \delta t \underline{\lambda}_m|} \|E_m\|_F < \frac{1}{3} \|E_m\|_F. \qquad \square$$

Lemma 4.2. *Assume that*

$$\alpha_m \equiv a_m \sqrt{n} \underline{\lambda}_m \underline{\lambda}_{m-1} - 3b(1 + 1/\sqrt{n}) > 0, \tag{21}$$

where $b \equiv \max_{1 \leq i \leq n} \|e_i^\top A\|_2$. *Then*

$$\frac{1}{\sqrt{n}} \|D_m^{-1/2} \left(A_m^{-1} - A_{m-1}^{-1}\right) \mathbf{f}^{(m-1)}\|_F < \frac{1}{3} \|E_m\|_F \tag{22}$$

for all

$$\delta t > T_2 \equiv \max \left\{ T_0, \frac{-\beta_m + \sqrt{\beta_m^2 - 4\alpha_m \gamma_m}}{2\alpha_m} \right\},$$

where T_0 *is defined in* (15) *and*

$$\beta_m = -a_m \sqrt{n} \left(\underline{\lambda}_m + \underline{\lambda}_{m-1}\right), \quad \gamma_m = a_m \sqrt{n}.$$

Proof. By the definition of A_m in (12), it holds that

$$\begin{aligned}
&\frac{1}{\sqrt{n}} D_m^{-1/2} \left(A_m^{-1} - A_{m-1}^{-1}\right) \mathbf{f}^{(m-1)} \\
&= \frac{1}{\sqrt{n}} D_m^{-1/2} A_m^{-1} \left(A_{m-1} - A_m\right) A_{m-1}^{-1} \mathbf{f}^{(m-1)} \\
&= \frac{\delta t}{\sqrt{n}} D_m^{-1/2} A_m^{-1} \left(\prec A\mathbf{f}^{(m)}, \mathbf{f}^{(m)} \succ - \prec A\mathbf{f}^{(m-1)}, \mathbf{f}^{(m-1)} \succ \right) A_{m-1}^{-1} \mathbf{f}^{(m-1)} \\
&= \frac{\delta t}{\sqrt{n}} D_m^{-1/2} A_m^{-1} \left(\prec A\mathbf{f}^{(m)}, E_m \succ + \prec AE_m, \mathbf{f}^{(m-1)} \succ \right) A_{m-1}^{-1} \mathbf{f}^{(m-1)}.
\end{aligned}$$

Since

$$\begin{aligned}
\| \prec A\mathbf{f}^{(m)}, E_m \succ \|_2 &\leq \max_i \|e_i^\top A\|_2 \|\mathbf{f}^{(m)}\|_F \|E_m\|_F \\
&= \max_i \|e_i^\top A\|_2 \|E_m\|_F \equiv b \|E_m\|_F
\end{aligned}$$

and

$$\begin{aligned}\| \prec AE_m, \mathbf{f}^{(m-1)} \succ \|_2 &= \max_i |\left(e_i^\top AE_m\right)\left(e_i^\top \mathbf{f}^{(m-1)}\right)^\top| \\ &\le \max_i \|e_i^\top AE_m\|_2 \max_i \|e_i^\top \mathbf{f}^{(m-1)}\|_2 \\ &\le \max_i \|e_i^\top A\|_2 \frac{1}{\sqrt{n}} \|E_m\|_F \equiv \frac{b}{\sqrt{n}} \|E_m\|_F,\end{aligned}$$

we have

$$\begin{aligned}&\frac{1}{\sqrt{n}} \|D_m^{-1/2}\left(A_m^{-1} - A_{m-1}^{-1}\right)\mathbf{f}^{(m-1)}\|_F \\ &\le \frac{(\delta t)^2}{\sqrt{n}} \frac{b + b/\sqrt{n}}{|1 - \delta t \underline{\lambda}_m| \cdot |1 - \delta t \underline{\lambda}_{m-1}| a_m} \|E_m\|_F \|\mathbf{f}^{(m-1)}\|_F \\ &= \frac{(\delta t)^2}{\sqrt{n}} \frac{b + b/\sqrt{n}}{|1 - \delta t \underline{\lambda}_m| \cdot |1 - \delta t \underline{\lambda}_{m-1}| a_m} \|E_m\|_F. \qquad (23)\end{aligned}$$

By the definitions of α_m, β_m and γ_m, it follows that

$$\beta_m^2 - 4\alpha_m\gamma_m = n a_m^2 \left(\underline{\lambda}_m - \underline{\lambda}_{m-1}\right)^2 + 12\sqrt{n} a_m b (1 + 1/\sqrt{n}) > 0.$$

Using the assumption $\alpha_m > 0$, for all $\delta t > T_2$, we have

$$\left(\delta t - \frac{-\beta_m + \sqrt{\beta_m^2 - 4\alpha_m\gamma_m}}{2\alpha_m}\right)\left(\delta t - \frac{-\beta_m - \sqrt{\beta_m^2 - 4\alpha_m\gamma_m}}{2\alpha_m}\right) > 0$$

which implies that

$$\sqrt{n} a_m \left[1 - \left(\underline{\lambda}_m + \underline{\lambda}_{m-1}\right)\delta t + \underline{\lambda}_m \underline{\lambda}_{m-1} (\delta t)^2\right] > 3b(1 + 1/\sqrt{n}) (\delta t)^2.$$

Consequently,

$$\frac{(\delta t)^2}{\sqrt{n}} \frac{b + b/\sqrt{n}}{|1 - \delta t \underline{\lambda}_m| \cdot |1 - \delta t \underline{\lambda}_{m-1}| a_m} < \frac{1}{3}. \qquad (24)$$

Substituting (24) into (23), the result in (22) is obtained. □

Lemma 4.3. *Assume that*

$$\min_{1 \le i \le n} \|q_{i,m}^\top \Lambda_m^{-1} Q_m^\top \mathbf{f}^{(m)}\|_2 > \eta_m, \qquad (25)$$

(26)
$$3\left(|\underline{\lambda}_m| + |\underline{\lambda}_{m-1}|\right)(b + b/\sqrt{n}) + 6|\underline{\lambda}_m\underline{\lambda}_{m-1}| < \sqrt{n}a_m a_{m-1}c_m\underline{\lambda}_m^2\underline{\lambda}_{m-1}^2|\underline{\lambda}_m|,$$

where η_m *is defined in* (15) *and*

$$c_m = \min_i \left(\|q_{i,m}^\top \Lambda_m^{-1} Q_m^\top \mathbf{f}^{(m)}\|_2 + \|q_{i,m-1}^\top \Lambda_{m-1}^{-1} Q_{m-1}^\top \mathbf{f}^{(m-1)}\|_2 - \eta_m - \eta_{m-1}\right).$$

Then there exists $T_3 > 0$ *such that*

$$\frac{1}{\sqrt{n}}\| \left(D_m^{-1/2} - D_{m-1}^{-1/2}\right) A_{m-1}^{-1}\mathbf{f}^{(m-1)}\|_F < \frac{1}{3}\|E_m\|_F$$

for $\delta t \geq T_3$.

Proof. We rewrite the third term on the right hand side of (17) as

$$\frac{1}{\sqrt{n}}\left(D_m^{-1/2} - D_{m-1}^{-1/2}\right) A_{m-1}^{-1}\mathbf{f}^{(m-1)}$$

(27)
$$= \frac{1}{\sqrt{n}}(D_m - D_{m-1})\left\{D_m^{-1/2}D_{m-1}^{-1/2}\left(D_m^{1/2} + D_{m-1}^{1/2}\right)^{-1}\right\} A_{m-1}^{-1}\mathbf{f}^{(m-1)}.$$

From (14) and (15), we have

$$\begin{aligned} w_i &\equiv e_i^\top \left(D_m^{1/2} + D_{m-1}^{1/2}\right) e_i \\ &= \frac{1}{\delta t}\left\{\|q_{i,m}^\top \Lambda_m^{-1} Q_m^\top \mathbf{f}^{(m)} + \mathcal{O}_m(\frac{1}{\delta t})\|_2 \right. \\ &\quad \left. + \|q_{i,m-1}^\top \Lambda_{m-1}^{-1} Q_{m-1}^\top \mathbf{f}^{(m-1)} + \mathcal{O}_{m-1}(\frac{1}{\delta t})\|_2\right\} \\ &\geq \frac{1}{\delta t}\left\{\|q_{i,m}^\top \Lambda_m^{-1} Q_m^\top \mathbf{f}^{(m)}\|_2 + \|q_{i,m-1}^\top \Lambda_{m-1}^{-1} Q_{m-1}^\top \mathbf{f}^{(m-1)}\|_2 - \eta_m - \eta_{m-1}\right\} \end{aligned}$$

for $\delta t \geq T_0$, which implies that

$$\begin{aligned} &\| \left(D_m^{1/2} + D_{m-1}^{1/2}\right)^{-1} \|_2 = \max_{1\leq i\leq n} w_i^{-1} = \left\{\min_{1\leq i\leq n} w_i\right\}^{-1} \\ &\leq \delta t\left\{\min_i \left(\|q_{i,m}^\top \Lambda_m^{-1} Q_m^\top \mathbf{f}^{(m)}\|_2 + \|q_{i,m-1}^\top \Lambda_{m-1}^{-1} Q_{m-1}^\top \mathbf{f}^{(m-1)}\|_2 - \eta_m - \eta_{m-1}\right)\right\}^{-1} \end{aligned}$$

(28)
$$\equiv \frac{\delta t}{c_m}.$$

On the other hand,

$$
\begin{aligned}
&D_m - D_{m-1} \\
=&\prec A_m^{-1}\mathbf{f}^{(m)}, A_m^{-1}\mathbf{f}^{(m)} \succ - \prec A_m^{-1}\mathbf{f}^{(m)}, A_m^{-1}\mathbf{f}^{(m)} \succ \\
=&\prec A_m^{-1}\mathbf{f}^{(m)}, (A_m^{-1} - A_{m-1}^{-1})\mathbf{f}^{(m)} \succ + \prec A_m^{-1}\mathbf{f}^{(m)}, A_{m-1}^{-1}E_m \succ \\
&+ \prec A_m^{-1}E_m, A_{m-1}^{-1}\mathbf{f}^{(m-1)} \succ + \prec (A_m^{-1} - A_{m-1}^{-1})\mathbf{f}^{(m-1)}, A_{m-1}^{-1}\mathbf{f}^{(m-1)} \succ .
\end{aligned} \tag{29}
$$

From (23), it follows that

$$
\|A_m^{-1} - A_{m-1}^{-1}\|_2 \leq \frac{(b + b/\sqrt{n})\delta t}{|1 - \delta t\underline{\lambda}_m| \cdot |1 - \delta t\underline{\lambda}_{m-1}|}\|E_m\|_F. \tag{30}
$$

From (18), (29) and (30) with the results $\|\mathbf{f}^{(m-1)}\|_F = \|\mathbf{f}^{(m)}\|_F = 1$, we have

$$
\begin{aligned}
&\|D_m - D_{m-1}\|_2 \\
\leq& \| \prec A_m^{-1}\mathbf{f}^{(m)}, (A_m^{-1} - A_{m-1}^{-1})\mathbf{f}^{(m)} \succ \|_2 + \| \prec A_m^{-1}\mathbf{f}^{(m)}, A_{m-1}^{-1}E_m \succ \|_2 \\
&+ \| \prec A_m^{-1}E_m, A_{m-1}^{-1}\mathbf{f}^{(m-1)} \succ \|_2 \\
&+ \| \prec (A_m^{-1} - A_{m-1}^{-1})\mathbf{f}^{(m-1)}, A_{m-1}^{-1}\mathbf{f}^{(m-1)} \succ \|_2 \\
\leq& (\|A_m^{-1}\|_2 + \|A_{m-1}^{-1}\|_2)\|A_m^{-1} - A_{m-1}^{-1}\|_2 + 2\|A_m^{-1}\|_2\|A_{m-1}^{-1}\|_2\|E_m\|_2 \\
\leq& \left(\frac{1}{|1 - \delta t\underline{\lambda}_m|} + \frac{1}{|1 - \delta t\underline{\lambda}_{m-1}|}\right)\frac{(b + b/\sqrt{n})\delta t}{|1 - \delta t\underline{\lambda}_m| \cdot |1 - \delta t\underline{\lambda}_{m-1}|}\|E_m\|_F \\
&+ \frac{2}{|1 - \delta t\underline{\lambda}_m| \cdot |1 - \delta t\underline{\lambda}_{m-1}|}\|E_m\|_F.
\end{aligned} \tag{31}
$$

Using (18), (28), (31) and the assumption (26), (27) implies that

$$
\begin{aligned}
&\frac{1}{\sqrt{n}}\| \left(D_m^{-1/2} - D_{m-1}^{-1/2}\right) A_{m-1}^{-1}\mathbf{f}^{(m-1)}\|_F \\
\leq& \frac{1}{\sqrt{n}}\|D_m - D_{m-1}\|_2\|D_m^{-1/2}\|_2\|D_{m-1}^{-1/2}\|_2\| \left(D_m^{1/2} + D_{m-1}^{1/2}\right)^{-1} \|_2\|A_{m-1}^{-1}\|_2 \\
\leq& \frac{1}{\sqrt{n}}\frac{\delta t}{a_m}\frac{\delta t}{a_{m-1}}\frac{1}{|1 - \delta t\underline{\lambda}_m|}\frac{\delta t}{c_m}\left\{\frac{2}{|1 - \delta t\underline{\lambda}_m| \cdot |1 - \delta t\underline{\lambda}_{m-1}|} + \right. \\
&\left.\left(\frac{1}{|1 - \delta t\underline{\lambda}_m|} + \frac{1}{|1 - \delta t\underline{\lambda}_{m-1}|}\right)\frac{(b + b/\sqrt{n})\delta t}{|1 - \delta t\underline{\lambda}_m| \cdot |1 - \delta t\underline{\lambda}_{m-1}|}\right\}\|E_m\|_F
\end{aligned}
$$

$$
\begin{aligned}
&= \frac{(\delta t)^3}{\sqrt{n} a_m a_{m-1} c_m (1-\delta t \underline{\lambda}_m)^2 |1-\delta t \underline{\lambda}_{m-1}|} \times \\
&\quad \left\{ 2 + \left(\frac{1}{|1-\delta t \underline{\lambda}_m|} + \frac{1}{|1-\delta t \underline{\lambda}_{m-1}|} \right) (b + b/\sqrt{n}) \delta t \right\} \\
&< \frac{1}{3} \|E_m\|_F, \qquad \text{(by the assumption (26))}
\end{aligned}
$$

for $\delta t \geq T_3$ with large enough T_3. □

Using the results in Lemmas 4.1, 4.2 and 4.3 into (17), we can easily show the decrease of the error $\|E_m\|_F$.

Theorem 4.1. *Assume that inequalities of* (19), (21), (25) *and* (26) *hold. Then there exists* $T > 0$ *such that*

$$\|E_m\|_F \equiv \|\mathbf{f}^{(m+1)} - \mathbf{f}^{(m)}\|_F < \|\mathbf{f}^{(m)} - \mathbf{f}^{(m-1)}\|_F \equiv \|E_{m-1}\|_F$$

for all $\delta t > T$.

Now, we consider a more simplified case for $\mathbf{f}^{(m)}$ and $\mathbf{f}^{(m+1)}$ without normalization. Assume

$$\|e_i^\top \mathbf{f}^{(m-1)}\|_2 = 1, \quad \text{for } i = 1, \ldots, n. \tag{32}$$

Let

$$\mathbf{f}^{(m)} = A_{m-1}^{-1} \mathbf{f}^{(m-1)}, \quad \mathbf{f}^{(m+1)} = A_m^{-1} \mathbf{f}^{(m)},$$

where A_m is defined in (12) and

$$
\begin{aligned}
\alpha_m &= \underline{\lambda}_{m-1} \underline{\lambda}_m, \\
\beta_m &= \underline{\lambda}_m + \underline{\lambda}_{m-1} + 4b\sqrt{n}.
\end{aligned}
$$

where $\underline{\lambda}_m$ is defined in (18). Then $f^{(m-1)}$, $f^{(m)}$ and $f^{(m+1)}$ satisfy the following result.

Theorem 4.2. *Assume* α_m, $\beta_m^2 - 4\alpha_m > 0$. *If* δt *satisfies that*

$$\delta t > \begin{cases} (\sqrt{n}+1)/\underline{\lambda}_m, & \text{if } \underline{\lambda}_m > 0; \\ (\sqrt{n}-1)/(-\underline{\lambda}_m), & \text{if } \underline{\lambda}_m < 0, \end{cases} \tag{33}$$

and

$$\delta t > \frac{\beta_m + \sqrt{\beta_m^2 - 4\alpha_m}}{2\alpha_m},$$

then $\|\mathbf{f}^{(m+1)} - \mathbf{f}^{(m)}\|_F < \|\mathbf{f}^{(m)} - \mathbf{f}^{(m-1)}\|_F$.

Proof. From (12), we have

$$\begin{aligned}
E_{m+1} &\equiv \mathbf{f}^{(m+1)} - \mathbf{f}^{(m)} = A_m^{-1}\mathbf{f}^{(m)} - A_{m-1}^{-1}\mathbf{f}^{(m-1)} \\
&= A_m^{-1}\mathbf{f}^{(m)} - A_m^{-1}\mathbf{f}^{(m-1)} + A_m^{-1}\mathbf{f}^{(m-1)} - A_{m-1}^{-1}\mathbf{f}^{(m-1)} \\
&= A_m^{-1}E_m + A_m^{-1}\left(A_{m-1} - A_m\right)A_{m-1}^{-1}\mathbf{f}^{(m-1)} \\
&= A_m^{-1}E_m + (\delta t)\,A_m^{-1}\Big(\prec A\mathbf{f}^{(m)}, \mathbf{f}^{(m)} \succ \\
&\quad - \prec A\mathbf{f}^{(m-1)}, \mathbf{f}^{(m-1)} \succ\Big)\,A_{m-1}^{-1}\mathbf{f}^{(m-1)} \\
&= A_m^{-1}E_m + (\delta t)\,A_m^{-1}\Big(\prec A\mathbf{f}^{(m)}, \mathbf{f}^{(m)} \succ - \prec A\mathbf{f}^{(m)}, \mathbf{f}^{(m-1)} \succ \\
&\quad + \prec A\mathbf{f}^{(m)}, \mathbf{f}^{(m-1)} \succ - \prec A\mathbf{f}^{(m-1)}, \mathbf{f}^{(m-1)} \succ\Big)\,A_{m-1}^{-1}\mathbf{f}^{(m-1)}. \qquad (34)
\end{aligned}$$

By Definition 3.1, it holds that

$$\begin{aligned}
&\| \prec A\mathbf{f}^{(m)}, \mathbf{f}^{(m-1)} \succ - \prec A\mathbf{f}^{(m-1)}, \mathbf{f}^{(m-1)} \succ \|_2 \\
&= \| \prec AE_m, \mathbf{f}^{(m-1)} \succ \|_2 = \max_{1\le i\le n}\left|e_i^\top AE_m\left(\mathbf{f}^{(m-1)}\right)^\top e_i\right|.
\end{aligned}$$

By the assumption in (32), we have

$$\begin{aligned}
&\| \prec A\mathbf{f}^{(m)}, \mathbf{f}^{(m-1)} \succ - \prec A\mathbf{f}^{(m-1)}, \mathbf{f}^{(m-1)} \succ \|_2 \\
&\le \max_{1\le i\le n}\|e_i^\top AE_m\|_2 \le \max_{1\le i\le n}\|e_i^\top A\|_2\|E_m\|_F \equiv b\|E_m\|_F. \qquad (35)
\end{aligned}$$

On the other hand, using $\mathbf{f}^{(m)} = A_m^{-1}\mathbf{f}^{(m-1)}$ and (12), (18) and (32), it holds that

$$\begin{aligned}
&\| \prec A\mathbf{f}^{(m)}, \mathbf{f}^{(m)} \succ - \prec A\mathbf{f}^{(m)}, \mathbf{f}^{(m-1)} \succ \|_2 \\
&= \max_{1\le i\le n}\left|e_i^\top AA_m^{-1}\mathbf{f}^{(m-1)}E_m^\top e_i\right| \\
&\le \max_{1\le i\le n}\|e_i^\top A\|_2\ \|A_m^{-1}\|_2\ \|\mathbf{f}^{(m-1)}\|_2\ \|E_m\|_F \\
&\le \frac{b\sqrt{n}}{|1 - \underline{\lambda}_m\delta t|}\|E_m\|_F. \qquad (36)
\end{aligned}$$

The assumption in (33) implies that

$$\frac{\sqrt{n}}{|1 - \underline{\lambda}_m\delta t|} < 1$$

and

$$\frac{1}{|1-\underline{\lambda}_m\delta t|} < \frac{1}{\sqrt{n}} < \frac{1}{2}, \quad \text{if } n > 4. \tag{37}$$

Consequently, from (36),

$$\| \prec A\mathbf{f}^{(m)}, \mathbf{f}^{(m)} \succ - \prec A\mathbf{f}^{(m)}, \mathbf{f}^{(m-1)} \succ \|_2 < b\|E_m\|_F. \tag{38}$$

From (34), (35) and (38), we get

$$\begin{aligned} \|E_{m+1}\|_F &< \|A_m^{-1}\|_2\|E_m\|_F + 2b\,(\delta t)\,\|A_m^{-1}\|_2\|A_{m-1}^{-1}\|_2\|\mathbf{f}^{(m-1)}\|_2\|E_m\|_F \\ &< \left\{\frac{1}{|1-\underline{\lambda}_m\delta t|} + \frac{2b\,(\delta t)\,\sqrt{n}}{|1-\underline{\lambda}_{m-1}\delta t|\;|1-\underline{\lambda}_m\delta t|}\right\}\|E_m\|_F. \end{aligned} \tag{39}$$

By the assumption that $\alpha_m,\ \beta_m^2 - 4\alpha_m > 0$, for all

$$\delta t > \frac{\beta_m + \sqrt{\beta_m^2 - 4\alpha_m}}{2\alpha_m},$$

we have

$$\left(\delta t - \frac{\beta_m + \sqrt{\beta_m^2 - 4\alpha_m}}{2\alpha_m}\right)\left(\delta t - \frac{\beta_m - \sqrt{\beta_m^2 - 4\alpha_m}}{2\alpha_m}\right) > 0$$

which implies that

$$\left[1 - \left(\underline{\lambda}_m + \underline{\lambda}_{m-1}\right)\delta t + \underline{\lambda}_m\underline{\lambda}_{m-1}\,(\delta t)^2\right] > 4b\sqrt{n}\delta t$$

and

$$\frac{2b\,(\delta t)\,\sqrt{n}}{|1-\underline{\lambda}_{m-1}\delta t|\;|1-\underline{\lambda}_m\delta t|} < \frac{1}{2}. \tag{40}$$

Substituting (37) and (40) into (39), it holds that $\|E_{m+1}\|_F < \|E_m\|_F$. □

5. Practical implementation

In this section, we shall discuss how to efficiently compute the steady-state solution of (7) with zero mass-center normalization by QIEM.

We remark that the QIEM algorithm is mainly used to compute conformal parameterization for regular meshes. For meshes with sharp tails,

some artificial foldings may happen in the iterative process. In this case, one can take some local refinement to remesh the region with sharp tails. Furthermore, if the artificial foldings still happen with mesh refinement or the refinement skill is not available, we recommend that one can switch to the efficient approach of the conformal correction proposed in [23] to remedy this drawback.

5.1. The initial mapping $\mathbf{f}^{(0)}$

For the spherical conformal mapping on genus-zero closed surfaces, the initial map $\mathbf{f}^{(0)}$ in (10) is to construct an one-to-one and onto smooth map from a given genus-zero closed surface to the unit sphere. In practice, we choose the Gauss map as the initial map $\mathbf{f}^{(0)}$, which is defined as follows:

Definition 5.1 (Gauss map)**.** $\mathcal{G} : M \to \mathbb{S}^2$, $\mathcal{G}(v) = \mathbf{n}(v)$, *where* $\mathbf{n}(v)$ *is the unit normal vector at* $v \in M$.

The corresponding Gauss map can be computed, for instance, as the weighted sum of normals on the adjacent faces weighed by their areas [25].

For the case of simply connected surfaces with a single boundary, i.e., computing the Riemann mapping, we use the idea described in [20] to construct a harmonic-type initial map. Specifically, we first parametrize the open surface onto a unit disk by the harmonic map. Using the stereographic projection, the resulting mesh is mapped to a lower hemisphere. Then the harmonic-type initial map is obtained by reflecting the hemisphere's image along the equatorial plane to built a full unit sphere.

For genus-0 closed surfaces, if the initial Gauss map is not a good one, one may first divide it into two meshes with the identical boundary and then perform the barycentric mapping for each of them with an appropriate weight, such as harmonic [26], mean value [6] or semi-cotangent [33]. Then, similar to the previous mentioned harmonic-type initialization for the Riemann mapping, we can get a better initial map.

5.2. Adaptive time step control

The convergence of solving the steady-state solution of the time-dependent differential equations with fixed time step δt may be very slow. In order to accelerate the convergence, we propose a time step controlling scheme to control δt in (10) for each iteration m. As a consequence, the sequence $\{\mathbf{f}^{(m)}\}$ can be convergent as soon as possible.

Let δt_0 be an initial time step determined by the strategy introduced in lines 1–5 of Algorithm 5.1 and $\delta t_{\max}$ denote the maximal time step so that δt is set to be $\delta t_{\max}$ if $\delta t > \delta t_{\max}$. The strategy of choosing δt in each iteration is based on the decrement of the harmonic energy $\mathcal{E}_h(\mathbf{f})$, i.e., the time steps are chosen such that the harmonic energy is always decreasing in each iteration. This objective can be achieved by the *descending* and *accelerating* strategies of time step controls. The descending strategy is used to determine δt so that $\mathcal{E}_h(\mathbf{f}^{(m+1)})$ is always decreasing, i.e., $\mathcal{E}_h(\mathbf{f}^{(m+1)}) - \mathcal{E}_h(\mathbf{f}^{(m)}) < \varepsilon$, in each $m = 0, 1, \ldots, k$ for some k and tolerance ε. Given ε, δt_0 and an increment α, we describe this strategy as follows.

($\mathbf{S_2}$.a): If $\mathcal{E}_h(\mathbf{f}^{(m+1)}) - \mathcal{E}_h(\mathbf{f}^{(m)}) \geq \varepsilon$, then we reduce δt to be $\delta t := \frac{1}{2}\delta t$ and recompute $\mathbf{f}^{(m+1)}$ from (10). This step prevents the sequence $\{\mathbf{f}^{(m)}\}$ converges to a map whose harmonic energy is a local extreme.

($\mathbf{S_2}$.b): If the new $\mathcal{E}_h(\mathbf{f}^{(m+1)})$ is still larger than $\mathcal{E}_h(\mathbf{f}^{(m)})$ when δt has been repeatedly reduced three times, then we reduce the initial δt_0 to be $\delta t_0 := \delta t_0/\alpha$ and restart the algorithm with $m = 0$.

The iteration in (10) with the descending strategy is repeated till $\mathcal{E}_h(\mathbf{f}^{(m+1)})$ is closed enough to $\mathcal{E}_h(\mathbf{f}^{(m)})$. After the descending strategy, the following accelerating strategy is used to increase δt and to speed up the convergence further.

($\mathbf{S_2}$.c): If $\mathcal{E}_h(\mathbf{f}^{(m+1)})$ satisfies that $|\mathcal{E}_h(\mathbf{f}^{(m+1)}) - \mathcal{E}_h(\mathbf{f}^{(m)})| < 10 \times |\mathcal{E}_h(\mathbf{f}^{(m)}) - \mathcal{E}_h(\mathbf{f}^{(m-1)})|$, then δt is increased by $\delta t := \min(\delta t_{\max}, \delta t \times \alpha)$; otherwise, δt need to be reduced by $\delta t := \delta t/\alpha$, and we recompute $\mathbf{f}^{(m+1)}$ from (10).

5.3. Two-phase quasi-implicit Euler method

To determine the initial map $\mathbf{f}^{(0)}$ in (10) is a crucial cornerstone to implement the QIEM for the evolution of conformal mappings on the unit sphere or on the unit disk. If $\mathbf{f}^{(0)}$ is not close to the steady-state solution, then it is difficult to find a large stable convergence region of the time steps for solving (7) by QIEM with time step controlling strategies (S_2.a), (S_2.b) and (S_2.c). To remedy this drawback, we propose a two-phase QIEM. If $\mathbf{f}^{(0)}$ is not close to the steady-state solution, the heuristic phase-I QIEM

$$\frac{\mathbf{f}^{(m+1)} - \mathbf{f}^{(m)}}{\delta t} = -\Delta_d \mathbf{f}^{(m+1)} = -A\mathbf{f}^{(m+1)},$$

i.e.,

$$(I + (\delta t)A)\,\mathbf{f}^{(m+1)} = \mathbf{f}^{(m)}$$

is used to compute $\mathbf{f}^{(m+1)}$. When $\mathbf{f}^{(m)}$ is close to the steady-state solution, we switch to (10) with strategies (S_2.a), (S_2.b) and (S_2.c) for computing $\mathbf{f}^{(m+1)}$, which we call the phase-II QIEM.

To set up a robust phase-I QIEM, we also propose an adaptive method, just as in the phase-II QIEM, to control δt in each iteration. The strategy described as follows is repeated until the difference $|\mathcal{E}_h(\mathbf{f}^{(m+1)}) - \mathcal{E}_h(\mathbf{f}^{(m)})|$ of the energy is less than a given tolerance ε_3.

(S_1.a): By the definition of A in (6), the row sums of A are equal to zero which implies that there is a trivial solution $\mathbf{f}$ such that $(A- \prec A\mathbf{f}, \mathbf{f} \succ)\,\mathbf{f} = 0$ and $\mathcal{E}_h(\mathbf{f}) = 0$. To avoid $\mathbf{f}^{(m)}$ convergent to this trivial solution, we reset δt_0 to be the current δt and restart the algorithm with the original $\mathbf{f}^{(0)}$ and new δt_0 when $\mathcal{E}_h(\mathbf{f}^{(m)})$ is less than a given small tolerance ε_2.

(S_1.b): If $\mathcal{E}_h(\mathbf{f}^{(m+1)})$ does not decrease, then we reduce δt to be $\delta t := \max(1, \frac{1}{2}\delta t)$ and recompute $\mathbf{f}^{(m+1)}$ from (10).

(S_1.c): If the difference of the energy is still larger than or equal to ε_3 when m has been larger than a given maximal iteration number $m_{\max}$, then we reset δt_0 to be the current δt and restart the algorithm with original initial closed surface $\mathbf{f}^{(0)}$ and new δt_0.

It is important to determine δt_0 for solving the steady-state problem. In general, the explicit Euler method has extremely narrow stability region of time steps which leads to the extremely slow convergence. The implicit Euler method has considerably wider stability region. However, it involves nonlinear systems that have to be solved by iterative solvers. If the time step is larger, then the initial guess of the iterative solver must be unrealistically close to the solution of the nonlinear systems. For two phases of QIEM, a heuristic method is proposed in Algorithm 5.1 to determine an initial time step. Comparing the initial time step in Algorithm 5.1 with those for the explicit and implicit Euler methods, our proposed time step is large. In Section 6, we numerically show that the proposed two phases of QIEM with an estimate initial time step in Algorithm 5.1 is highly efficient.

6. Numerical results

In this section, we conduct numerical experiments to evaluate the performances of the computation of Riemann and sphere conformal mappings. All

Algorithm 5.1 Two-phase quasi-implicit Euler method

Input: A genus zero triangular mesh M, an initial map $\mathbf{f}^{(0)}$ with the harmonic energy $\mathcal{E}_h(\mathbf{f}^{(0)})$ and a threshold δE for the energy difference.

Output: Convergent steady-state solution $\mathbf{f}^{(m)}$ with zero mass center.

1: Compute the areas $\mathcal{A}_i$, $i = 1, \ldots, n$, of all faces in M;
2: Resort $\mathcal{A}_i$ for $i = 1, \ldots, n$;
3: Compute the average $\mathcal{A}$ of the areas $\mathcal{A}_i$ for $i = 0.45n, \ldots, 0.55n$;
4: Find the minimal positive integer k such that $\mathcal{A}^{k/3-7} \leq 3500$.
5: Compute $\delta t_0 = \mathcal{A}^{k/3-7}$.
6: **if** $\mathbf{f}^{(0)}$ is not close to the steady-state solution **then**
7: **repeat**
8: Solve the linear system

$$(I + (\delta t)A)\,\mathbf{f}^{(m+1)} = \mathbf{f}^{(m)}.$$

9: Compute the mass sphere center $\mathbf{c}$:

$$\mathbf{c} = \left(\sum_{i=1}^{n} \mathcal{A}(v_i)\right)^{-1} \begin{bmatrix}\mathcal{A}(v_1) & \cdots & \mathcal{A}(v_n)\end{bmatrix} \mathbf{f}^{(m+1)}, \tag{41}$$

where $\mathcal{A}(v_i)$ is the sum of areas for the faces which have the common vertex $v_i, i = 1, \ldots, n$;
10: Normalize $\mathbf{f}^{(m+1)}$ by $(\mathbf{f}^{(m+1)} - \mathbf{c})/\|\mathbf{f}^{(m+1)} - \mathbf{c}\|$ such that the mass center of the resulting $\mathbf{f}^{(m+1)}$ is at the unit sphere center;
11: Compute δt according to strategies (S_1.a), (S_1.b) and (S_1.c) with $m_{\max} = 10$, $\varepsilon_2 = 0.5$ and $\varepsilon_3 = 0.1$;
12: **until** $|\mathcal{E}_h(\mathbf{f}^{(m+1)}) - \mathcal{E}_h(\mathbf{f}^{(m)})| < 0.1$
13: Set $\mathbf{f}^{(0)} = \mathbf{f}^{(m+1)}$ and $m = 0$;
14: **end if**
15: **repeat**
16: Solve the linear system

$$\left\{I + \delta t \left(A - \prec A\mathbf{f}^{(m)}, \mathbf{f}^{(m)} \succ\right)\right\} \mathbf{f}^{(m+1)} = \mathbf{f}^{(m)}.$$

17: Compute the mass sphere center $\mathbf{c}$ in (41);
18: Normalize $\mathbf{f}^{(m+1)}$ by $(\mathbf{f}^{(m+1)} - \mathbf{c})/\|\mathbf{f}^{(m+1)} - \mathbf{c}\|$ such that the mass center of the resulting $\mathbf{f}^{(m+1)}$ is at the unit sphere center;
19: Compute δt according to strategies (S_2.a), (S_2.b) and (S_2.c) with $\alpha = 1.05$ and $\varepsilon = 0.05$;
20: **until** $|\mathcal{E}_h(\mathbf{f}^{(m+1)}) - \mathcal{E}_h(\mathbf{f}^{(m)})| < \delta E$

Table 1: #V and #F denote the numbers of vertices and faces of M, respectively. dim is the dimension of the matrix A

Figure	#F	#V	dim	Figure	#F	#V	dim
1(a)	102256	51596	102258	2(a)	1005146	502575	502575
1(b)	135766	68430	135768	2(b)	858180	429092	429092
1(c)	136513	68802	136515	2(c)	284692	142348	142348
1(d)	127265	64156	127267	2(d)	39698	19851	19851
1(e)	127132	64095	127134				
1(f)	130560	65802	130562				
1(g)	140352	70720	140354				
1(h)	139198	70180	139200				

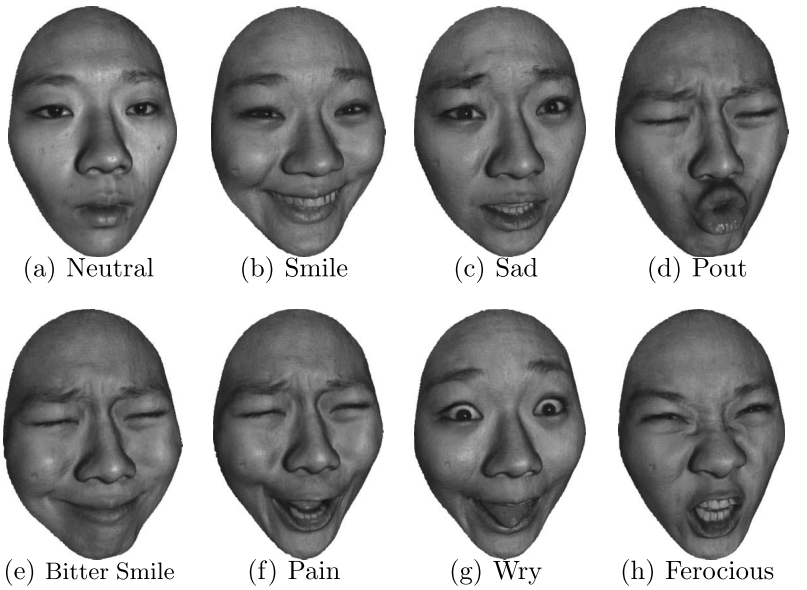

(a) Neutral (b) Smile (c) Sad (d) Pout

(e) Bitter Smile (f) Pain (g) Wry (h) Ferocious

Figure 1: The eight different facial expressions of one person.

computations are carried out in MATLAB 2011b on a HP workstation with two Intel Quad-Core Xeon X5687 3.6GHz CPUs, 48 GB main memory and RedHat Linux operation system, using IEEE double-precision floating-point arithmetic.

The benchmark problems come from the eight different facial expressions for a person in Figure 1 and four different genus zero closed surfaces in Figure 2, respectively. The corresponding mesh data are listed in Table 1.

Furthermore, we adapt the quasi-conformal (QC) distortion [27] to quantitatively measure the conformality (angle-preserving) of Riemann mappings

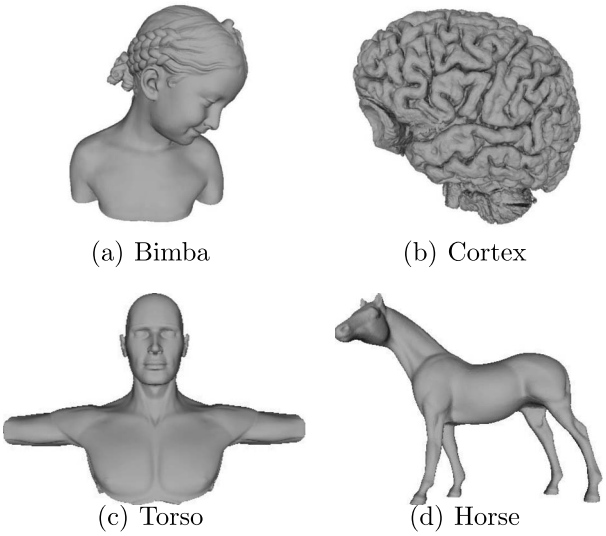

(a) Bimba (b) Cortex

(c) Torso (d) Horse

Figure 2: The four different genus zero closed surfaces.

for models in Figure 1. The ideal conformality is 1, and larger value are worse conformality. The parameterization results as well as the distribution of QC distortions for each experiment are presented in Figure 3. On the other hand, for the spherical conformal mappings, we directly compute the angle differences between triangles on the surfaces models in Figure 2 and the corresponding ones on the unit sphere. The frequency histograms of angle differences are shown in Figure 4.

As shown in the histograms of Figure 3 as well as Figure 4, we see that most of the QC distortions for Riemann mappings are close to 1 and most of the angle differences for the spherical conformal mappings are close to 0, these demonstrate that the conformality for the obtained maps is promising and satisfactory.

6.1. Efficiency of computing Riemann mapping by Algorithm 5.1

In this subsection, we demonstrate the efficiency of Algorithm 5.1 in solving the nonlinear heat diffusion equation (7) with zero mass center by (i) comparing the efficiency of the explicit, implicit and quasi-implicit Euler methods, (ii) robustness in choosing initial time step and (iii) high performance computing for the benchmark human faces in Figure 1. In (i) and (ii), we use the human face in Figure 1(a) as the benchmark problem. The stopping tolerance δE is taken as 10^{-9}. The initial map $\mathbf{f}^{(0)}$ are all constructed

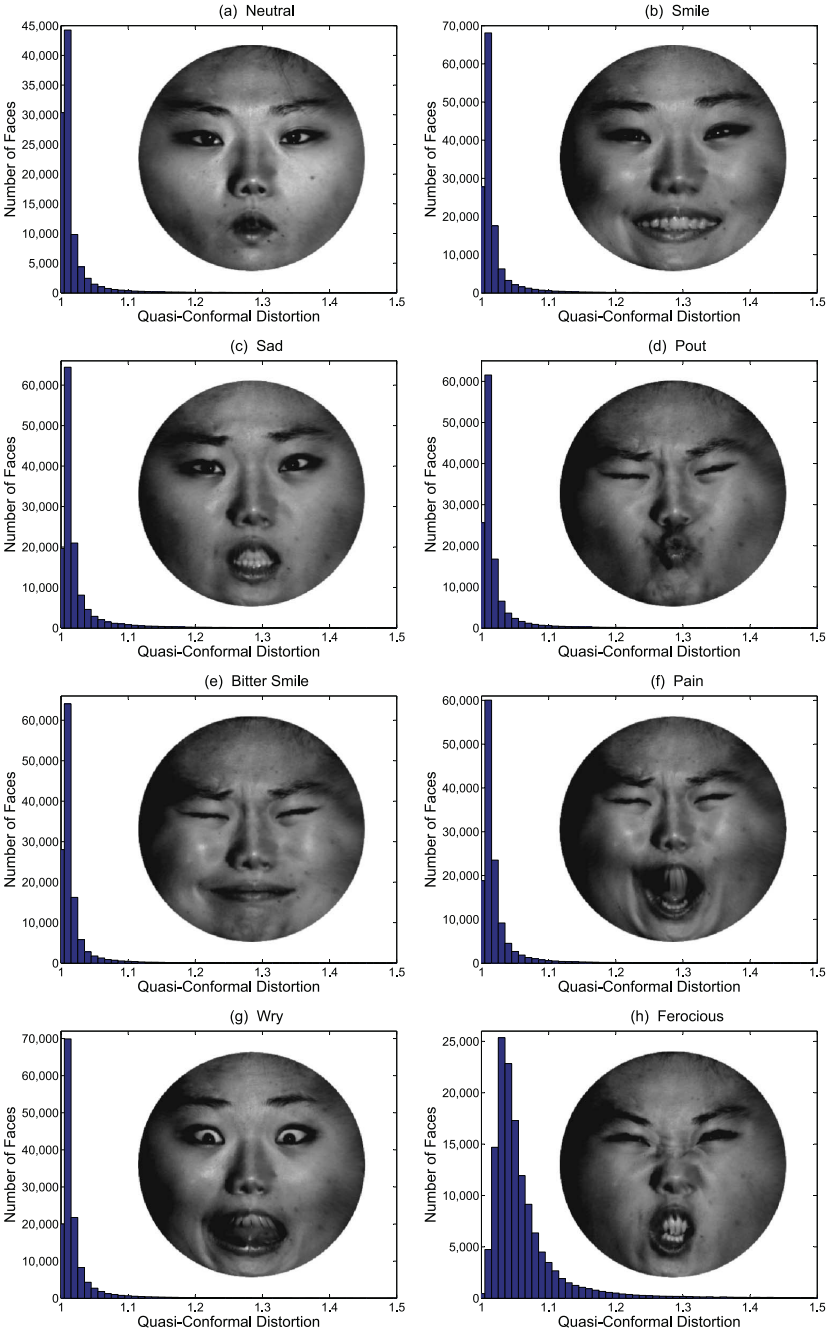

Figure 3: The Riemann mapping results and measurements of quasi-conformal distortion for mesh models in Figure 1.

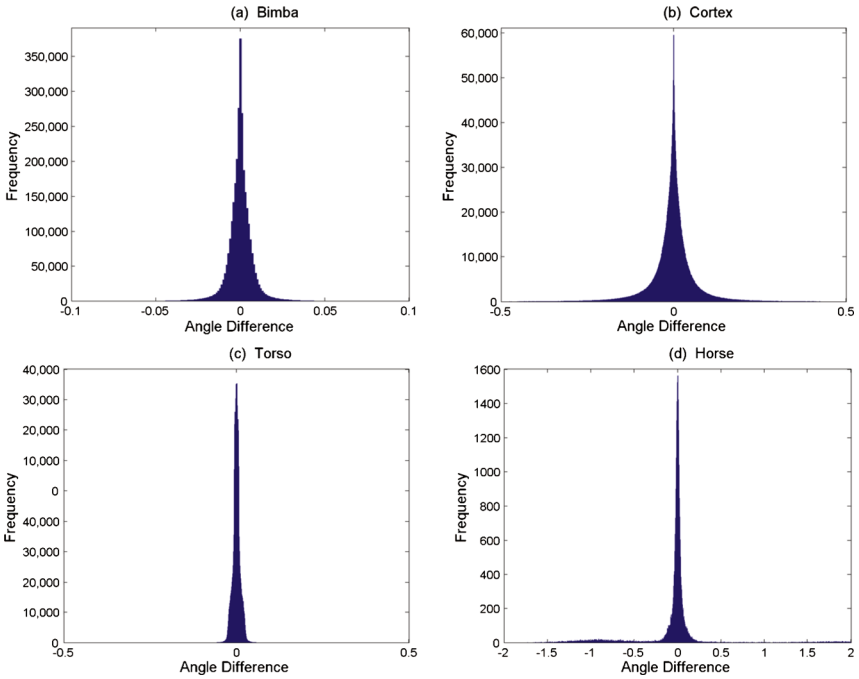

Figure 4: Angle difference histograms of spherical conformal mapping for mesh models in Figure 2.

by the harmonic-type initial map (see Section 5.1). Such $\mathbf{f}^{(0)}$ is close to the steady-state solution so that the phase-I QIEM, i.e., lines 7–13, is skipped in Algorithm 5.1. Only phase-II QIEM, i.e., lines 15–20, is used to compute the steady-state solution.

For each experiment, the initial δt_0's are chosen as large as possible in order to accelerate the convergence of each method. In particular, for the QIEM method, we determine the initial time δt_0 through the technique introduced in Section 5.2.

- **Comparison for the explicit, implicit and quasi-implicit Euler methods**: The initial time steps δt_0 for the explicit, implicit and quasi-implicit Euler methods are set to 0.003, 5 and 2881.05, respectively. For explicit Euler method, $\delta t = \delta t_0$ is fixed in each iteration. In order to accelerate the convergence of the implicit Euler method, we apply an adaptive method to control time step. The energy $\mathcal{E}_h(\mathbf{f}^{(m)})$ produced by Algorithm 5.1 is strictly monotonically decreasing so that $\delta t = \delta t_0$ is fixed at each iteration. The numerical results of the explicit, implicit

Table 2: Efficiency comparison

	Explicit Euler	Implicit Euler	QIEM
δt	0.003	5	2,881.05
#it	2,412,000	108	10
CPU time (sec.)	113,911.89	5,554.88	4.23

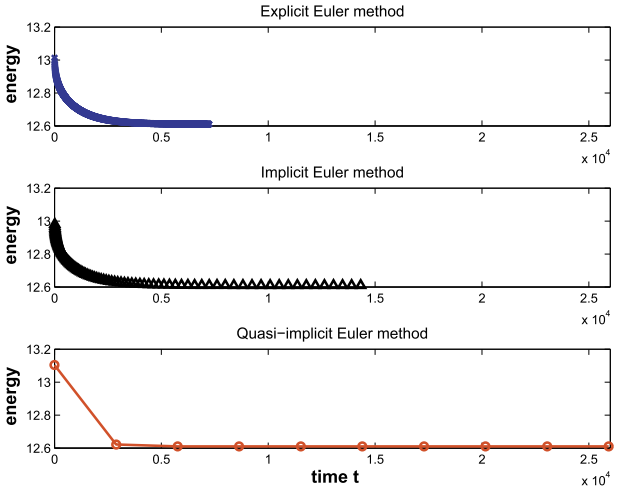

Figure 5: Convergence behavior of the computed harmonic energy produced by explicit, implicit and quasi-implicit Euler methods.

and quasi-implicit Euler methods are shown in Table 2. The notation #it in Table 2 denotes the total iteration number used to compute the solution. The convergence behaviors for these three methods are shown in Figure 5. From these numerical results, we see that the QIEM outperforms the explicit and implicit Euler methods greatly.

- **Robustness of choosing initial time step in Algorithm 5.1**: The numerical results have validated that the QIEM with the time step $\delta t = 2881.05$, which is estimated by Algorithm 5.1, outperforms the other two methods by big margins. Now, we demonstrate the robustness of Algorithm 5.1 with the harmonic-type initial map $\mathbf{f}^{(0)}$ for solving (7) with the human face in Figure 1(a). Four different initial time steps δt_0, namely (1, 10, 100, 1000), are applied to solve the steady-state problem and the maximum $\delta t_{\max}$ of time steps is equal to 2881.05. The associated numerical results are shown in Table 3 and the convergence behaviors of the harmonic energy are shown in Figure 6. The notation δt_{end} in Table 3 denotes the time step at the final itera-

Table 3: Numerical results for Algorithm 5.1 with different initial time step δt_0

δt_0	1	10	100	1000
δt_{end}	467.6	495.6	579.2	1551
#it	129	83	39	13
CPU time (sec.)	52.4	33.9	16.1	5.63

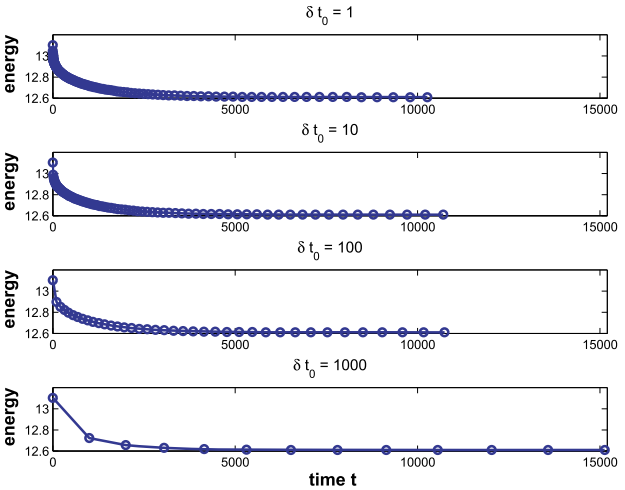

Figure 6: Convergence behavior of the computed harmonic energy produced by the phase-II quasi-implicit Euler method with different initial time step δt_0.

tion. The results in Table 3 and Figure 6 show that no matter which initial time step is used, the adaptive controlling processes in Algorithm 5.1 performs well. The time step in each iteration is effectively increasing and the convergence of the solution is accelerated. Furthermore, these results also show that the QIEM with a harmonic-type initial $\mathbf{f}^{(0)}$ has a wide stability region and the process of estimating time step in Algorithm 5.1 provides a near optimal initial time step.

The adaptive controlling time step is not only robust for the human face problems but also for other benchmark problems. Figure 7(b) presents the numerical results for applying Algorithm 5.1 to compute the Riemann mapping of the human hand in Figure 7(a). As shown in Figure 7(b), the time step is reduced from 3348.76 to 837.19 at the fourth iteration and then gradually increased to 3348.7. At the 41st iteration, it is again reduced to 1518.71 so that the harmonic energies

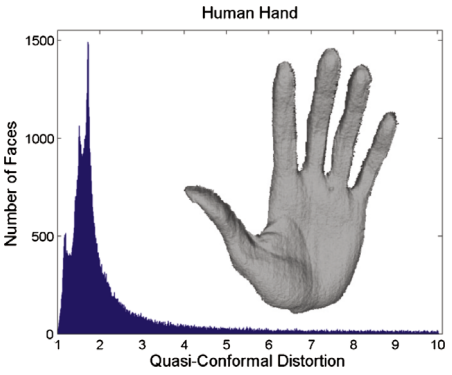

(a) Human hand

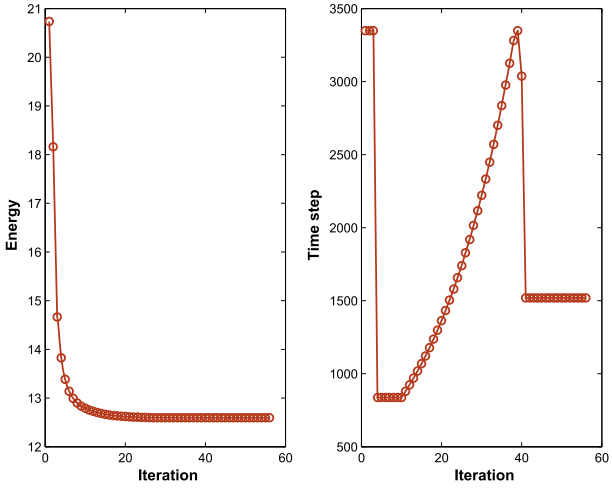

(b) Harmonic energies and time steps

Figure 7: The computed harmonic energies and time steps in each iteration of phase-II QIEM for the human hand.

are always decreasing. In each iteration, the time step is kept greater than or equal to 837.19 such that it only requires 56 iterations and 103.3 seconds to compute the Riemann mapping.

We remark that the parameterization result for the human hand model has a large QC distortion as in Figure 7(a). The main reason is that the shape of the human hand model is not suitable for fixed-boundary parameterization on the unit disc. The primary intention of presenting this experiment here is to show the advantages of the adaptive time step controlling.

Table 4: Numerical results for the benchmark problems produced by Algorithm 5.1 with harmonic-type initial map $\mathbf{f}^{(0)}$

Figure	δt_0	#it	t_c (sec.)	Figure	δt_0	#it	t_c (sec.)
1(a)	2881.1	10	4.23	1(e)	2155.6	10	5.46
1(b)	3377.7	8	4.80	1(f)	3307.4	15	8.11
1(c)	3375.1	7	4.34	1(g)	2102.3	13	8.08
1(d)	2890.6	11	6.02	1(h)	3474.0	11	16.9

- **High performance computing for Algorithm 5.1**: We demonstrate the high performance computing for Algorithm 5.1 with harmonic-type initial map $\mathbf{f}^{(0)}$ in solving the benchmark problems in Figure 1. The numerical results are shown in Table 4. The notation t_c in the table denotes the total CPU time for computing the conformal map by Algorithm 5.1. From Table 4, Algorithm 5.1 provides a large initial time step δt_0. Using such δt_0, it only needs $7 \sim 15$ iterations in Algorithm 5.1 to compute the steady-state solution of (7). The associated CPU times are less than 17 seconds for Figure 1, which illustrates the high performance of Algorithm 5.1.

6.2. Efficiency of Algorithm 5.1 for computing spherical conformal mapping

We have numerically illustrated the high performance of Algorithm 5.1 in computing Riemann mapping. In this subsection, we demonstrate the importance of phase-I QIEM in computing spherical conformal mapping and then show the performance for Algorithm 5.1 in solving the benchmark problems in Figure 2.

- **Effect of phase-I QIEM**: We compare the efficiency of the phase-II QIEM and Algorithm 5.1 for solving (7) with genus zero closed surface in Figure 2(c). The numerical results produced by Algorithm 5.1 are shown in Figure 8. Since the initial map $\mathbf{f}^{(0)}$ is far away from the steady-state solution, in our numerical experiences, it is difficult to find an initial time step such that the phase-II QIEM can be convergent. The stability region of the time step in the phase-II QIEM for computing spherical conformal mapping is extremely limited. On the contrary, Algorithm 5.1 with initial time step $\delta t_0 = 2077.71$ only requires 41 iterations which obviously outperforms phase-II QIEM. That is the phase-I QIEM in Algorithm 5.1 plays an important role in computing spherical conformal mapping.

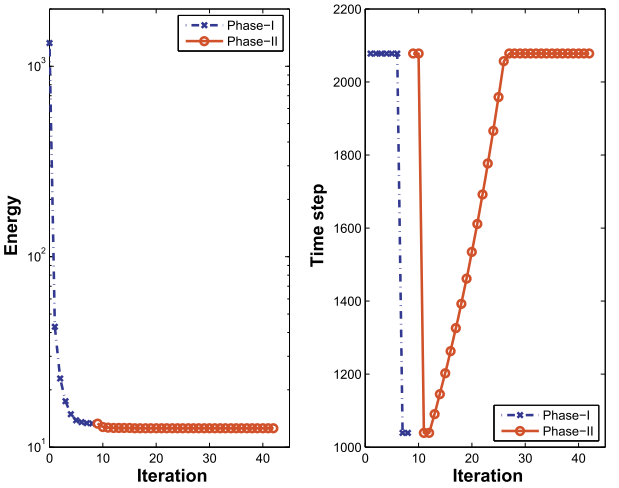

Figure 8: The computed harmonic energies and time steps in each iteration of the two-phase QIEM for the human torso in Figure 2(c).

Table 5: Numerical results for the benchmark problems in Figure 2 produced by Algorithm 5.1

Figure	$\#\text{it}_I$	$\#\text{it}_{II}$	t_c (sec.)	Figure	$\#\text{it}_I$	$\#\text{it}_{II}$	t_c (sec.)
2(a)	16	42	145.7	2(b)	8	121	234.6
2(c)	8	33	31.03	2(d)	5	80	6.117

- **Performance of Algorithm 5.1**: We demonstrate the high performance computing of Algorithm 5.1 in computing spherical conformal mapping for the benchmark problems in Figure 2. The numerical results are shown in Table 5. The notations $\#\text{it}_I$ and $\#\text{it}_{II}$ denote the total iteration numbers for phase-I and phase-II QIEMs, respectively. From the results in this table, we conclude that Algorithm 5.1 possesses high performance for computing the spherical conformal maps of genus zero closed surfaces.

7. Conclusions

For genus zero closed surfaces, a mapping is conformal if and only if it is harmonic. A traditional way to find the harmonic map is to minimize the harmonic energy by the time evolution according to the nonlinear heat diffusion (7). For this, we propose an efficient quasi-implicit Euler method (QIEM), and apply it to compute conformal mappings from a genus zero

closed surface to the unit sphere $\mathbb{S}^2$ (the spherical conformal mapping) as well as from a simply connected surface with a single boundary to a 2D disk $\mathbb{D}$ (the Riemann mapping). Furthermore, we analyze the convergence of the QIEM under some simplifications. In order to accelerate the convergence of this method, we develop a variant time step scheme and a heuristic method to determine an initial time step. Numerical results validate that the proposed algorithms possess high performance for computing the Riemann mapping. For the spherical conformal map, we propose a two-phase QIEM. In phase-I QIEM, the normal component of $\Delta_d \mathbf{f}$ is omitted to accelerate the computed map close to the steady-state solution as soon as possible. When the computed map is close to the steady-state solution in phase-I QIEM, we switch it to the phase-II QIEM. Numerical results confirm that the two-phase QIEM also possesses high performance for computing the spherical conformal map.

Acknowledgments

This work is partially supported by the ST Yau Center of the National Chiao Tung University, the National Science Council and the National Center for Theoretical Sciences in Taiwan.

Appendix

Here, we derive the Jacobian matrix $J(\mathbf{f}^{(m+1)})$ in (9) as follows. Let $f_k = [f_{1k}, \cdots, f_{nk}]^\top$ for $k = 1, 2, 3$. By Definition 3.1, it holds that, for $k = 1, 2, 3$,

$$\begin{aligned}(\prec A\mathbf{f}, \mathbf{f} \succ f_k)_i &= e_i^\top A[f_1, f_2, f_3][f_{i1}, f_{i2}, f_{i3}]^\top f_{ik} \\ &= e_i^\top A\left(f_{i1}f_1 + f_{i2}f_2 + f_{i3}f_3\right) f_{ik} \\ &= e_i^\top A\left(f_{ik}^2 f_k + \sum_{\ell \neq k} f_{ik} f_{i\ell} f_\ell\right) \\ &\equiv g_{ik}. \end{aligned} \tag{42}$$

It implies that, for $j \neq i$,

$$\frac{\partial g_{ik}}{\partial f_{jk}} = \frac{\partial}{\partial f_{jk}}\left(f_{ik}^2 e_i^\top A f_k\right) = a_{ij} f_{ik}^2,$$

where e_i is the ith column of the identity matrix, and

$$\frac{\partial g_{ik}}{\partial f_{ik}} = e_i^\top A\left(f_{i1}f_1 + f_{i2}f_2 + f_{i3}f_3\right) + f_{ik}\frac{\partial}{\partial f_{ik}}\left(f_{ik} e_i^\top A f_k\right)$$

$$
\begin{aligned}
&= e_i^\top A\left(f_{i1}f_1 + f_{i2}f_2 + f_{i3}f_3\right) + f_{ik}e_i^\top A f_k + f_{ik}^2 a_{ii} \\
&= e_i^\top A\left(f_{i1}f_1 + f_{i2}f_2 + f_{i3}f_3 + f_{ik}f_k\right) + f_{ik}^2 a_{ii} \\
&\equiv e_i^\top A h_k^{(i)} + f_{ik}^2 a_{ii}.
\end{aligned}
$$

Consequently,

$$
\begin{bmatrix} \frac{\partial g_{ik}}{\partial f_{1k}} & \frac{\partial g_{ik}}{\partial f_{2k}} & \cdots & \frac{\partial g_{ik}}{\partial f_{nk}} \end{bmatrix} = f_{ik}^2 e_i^\top A + \left(e_i^\top A h_k^{(i)}\right) e_i^\top
$$

and

$$
\begin{bmatrix} \frac{\partial g_{1k}}{\partial f_{1k}} & \cdots & \frac{\partial g_{1k}}{\partial f_{nk}} \\ \vdots & & \vdots \\ \frac{\partial g_{nk}}{\partial f_{1k}} & \cdots & \frac{\partial g_{nk}}{\partial f_{nk}} \end{bmatrix} = D_{k,f}^2 A + D_{k,h}, \tag{43}
$$

where $D_{k,f} = \operatorname{diag}(f_{1k}, f_{2k}, \cdots, f_{nk})$ and

$$
D_{k,h} = \operatorname{diag}\left(e_1^\top A h_k^{(1)}, e_2^\top A h_k^{(2)}, \cdots, e_n^\top A h_k^{(n)}\right).
$$

From (42), we have, for $\ell \neq k$,

$$
\frac{\partial g_{ik}}{\partial f_{j\ell}} = a_{ij} f_{ik} f_{i\ell}, \quad \text{for } j \neq i;
$$

and

$$
\frac{\partial g_{ik}}{\partial f_{i\ell}} = f_{ik} e_i^\top A f_\ell + f_{ik} f_{i\ell} a_{ii},
$$

which implies that

$$
\begin{bmatrix} \frac{\partial g_{ik}}{\partial f_{1\ell}} & \frac{\partial g_{ik}}{\partial f_{2\ell}} & \cdots & \frac{\partial g_{ik}}{\partial f_{n\ell}} \end{bmatrix} = f_{ik} f_{i\ell} e_i^\top A + \left\{f_{ik} e_i^\top A f_\ell\right\} e_i^\top
$$

and

$$
\begin{bmatrix} \frac{\partial g_{1k}}{\partial f_{1\ell}} & \cdots & \frac{\partial g_{1k}}{\partial f_{n\ell}} \\ \vdots & & \vdots \\ \frac{\partial g_{nk}}{\partial f_{1\ell}} & \cdots & \frac{\partial g_{nk}}{\partial f_{n\ell}} \end{bmatrix} = D_{k,f} D_{\ell,f} A + D_{k,\ell} \tag{44}
$$

with

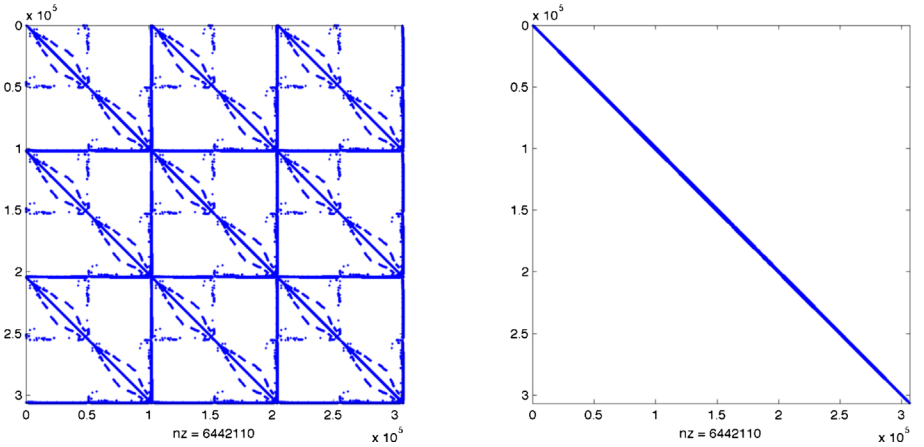

(a) Without permutation (b) With column and row permutations

Figure 9: Sparsity of the Jacobian matrix $J(\mathbf{f}_i^{(m+1)})$.

$$D_{k,\ell} = \operatorname{diag}\left(f_{k1}e_1^\top A f_\ell, \cdots, f_{kn}e_n^\top A f_\ell\right).$$

From (43) and (44), the Jacobian matrix $J_1(\mathbf{f})$ of $(I_3 \otimes \prec A\mathbf{f}, \mathbf{f} \succ)\operatorname{vec}(\mathbf{f})$ can be represented as

$$J_1(\mathbf{f}) = \begin{bmatrix} D_{1,f}^2 A + D_{1,h} & D_{1,f}D_{2,f}A + D_{1,2} & D_{1,f}D_{3,f}A + D_{1,3} \\ D_{2,f}D_{1,f}A + D_{2,1} & D_{2,f}^2 A + D_{2,h} & D_{2,f}D_{3,f}A + D_{2,3} \\ D_{3,f}D_{1,f}A + D_{3,1} & D_{3,f}D_{2,f}A + D_{3,2} & D_{3,f}^2 A + D_{3,h} \end{bmatrix}.$$

Therefore, the Jacobian matrix $J(\mathbf{f}^{(m+1)})$ is equal to

$$J\left(\mathbf{f}^{(m+1)}\right) = I_3 \otimes [I + (\delta t)A] - (\delta t)J_1(\mathbf{f}^{(m+1)}).$$

The sparsities of $J\left(\mathbf{f}^{(m+1)}\right)$ without/with column and row permutations are shown in Figure 9.

References

[1] P. Alliez, M. Meyer, and M. Desbrun. Interactive geometry remeshing. In *Comput. Graphics (Proc. SIGGRAPH 02)*, pp. 347–354, 2002.

[2] S. Angenent, S. Haker, A. Tannenbaum, and R. Kikinis. Conformal geometry and brain flattening. In *Proc. MICCAI*, 1999.

[3] M. Desbrun, M. Meyer, and P. Alliez. Intrinsic parameterizations of surface meshes. In *Proc. Eurographics*, pp. 210–218, 2002.

[4] L. Diening, A. Prohl, and Ružička. Semi-implicit Euler scheme for generalized Newtonian fluids. *SIAM J. Numer. Anal.*, 44:1172–1190, 2006. MR2231860

[5] M. Eck, T. DeRose, T. Duchamp, H. Hoppe, M. Lounsbery, and W. Stuetzle. Multiresolution analysis of arbitary meshes. In *Proc. of SIGGRAPH*, 1995, 173–182.

[6] M. S. Floater. Mean value coordinates. *Comput. Aided Geom. Des.*, 20:19–27, 2003. MR1968304

[7] K. R. Fowler and C. T. Kelley. Pseudo-transient continuation for non-smooth nonlinear equations. *SIAM J. Numer. Anal.*, 43:1385–1406, 2006. MR2182133

[8] P. Groisman. Totally discrete explicit and semi-implicit Euler methods for a blow-up problem in several space dimensions. *Computing*, 76:325–352, 2006. MR2210101

[9] X. Gu, Y. Wang, T. F. Chan, P. M. Thompson, and S.-T. Yau. Genus zero surface conformal mapping and its application to brain surface mapping. *IEEE Trans. Med. Imaging*, 23:949–958, 2004.

[10] X. Gu, Y. Wang, and S.-T. Yau. Computing conformal invariants: Period matrices. *Commun. Inf. Syst.*, 3:153–170, 2004. MR2131878

[11] X. Gu and S.-T. Yau. Computing conformal structures of surfaces. *Commun. Inform. Syst.*, 2:121–146, 2002. MR1958012

[12] X. Gu and S.-T. Yau. Global conformal surface parameterization. In *ACM Symposium on Geometry Processing*, 2003.

[13] X. Gu and S.-T. Yau. Surface classification using conformal structures. In *International Conference on Computer Vision*, 2003.

[14] X. D. Gu and S.-T. Yau. *Computational Conformal Geometry*. International Press of Boston, 2008. MR2439718

[15] S. Haker, S. Angenent, A. Tannenbaum, R. Kikinis, G. Sapiro, and M. Halle. Conformal surface parameterization for texture mapping. *IEEE Trans. Visual. Comput. Graphics*, 6:181–189, 2000.

[16] N. Hofmann, T. Müller-Gronbach, and K. Ritter. Optimal approximation of stochastic differential equations by adaptive step-size control. *Math. Comp.*, 69:1017–1034, 1999. MR1677407

[17] K. Hormann. *Theory and Applications of Parameterizing Triangulations*. PhD thesis, University of Erlangen, Germany, 2001.

[18] M. Hurdal, P. Bowers, K. Stephenson, D. Sumners, K. Rehm, K. Schaper, and D. Rottenberg. Quasiconformally flat mapping the human cerebellum. In *Lecture Notes in Computer Science*. Berlin, Germany: Springer-Verlag, vol. 1679, Proc. MICCAI'99, pp. 279–286, 1999.

[19] M. Hurdal, K. Stephenson, P. Bowers, D. Sumners, and D. Rottenberg. Coordinate systems for conformal cerebellar flat maps. *NeuroImage*, 11:S467, 2000.

[20] M. Isenburg, S. Gumholdy, and C. Gotsman. Connectivity shapes. In *IEEE Computer Society (Proc. of IEEE Visualization 2001)*, pp. 135–142, 2001.

[21] T. Kanai, H. Suzuki, and F. Kimura. Three-dimensional geometric metamorphosis based on harmonic maps. *Visual Comput.*, 14:166–176, 1998.

[22] C. T. Kelley and D. E. Keyes. Convergence analysis of pseudo-transient continuation. *SIAM J. Numer. Anal.*, 35:508–523, 1998. MR1618838

[23] R. Lai, Z. Wen, W. Yin, X. F. Gu, and L. M. Lui. Fast and accurate algorithms for harmonic energy minimization on genus-0 surfaces. *Journal of Scientific Computing*, 2013, accepted.

[24] B. Lévy, S. Petitjean, N. Ray, and J. Maillot. Least squares conformal maps for automatic texture atlas generation. In *Comput. Graphics (Proc. SIGGRAPH 02)*, 2002.

[25] X. Li, X. Gu, and H. Qin. Curve space: Classifying curves on surfaces. *Commun. Inf. Syst.*, 3:207–226, 2007. MR2516241

[26] U. Pinkall and K. Polthier. Computing discrete minimal surfaces and their conjugates. *Exp. Math.*, 2:15–36, 1993. MR1246481

[27] P. V. Sander, J. Snyder, S. J. Gortler, and H. Hoppe. Texture mapping progressive meshes. In *Proceedings of the 28th annual conference on Computer graphics and interactive techniques*, SIGGRAPH '01, pages 409–416, New York, NY, USA, 2001. ACM.

[28] A. Sheffer and E. de Sturler. Parameterization of faceted surfaces for meshing using angle-based flattening. *Eng. with Comput.*, 17:326–337, 2001.

[29] A. Sheffer, B. Lévy, M. Mogilnitsky, and A. Bogomyakov. Abf++: fast and robust angle based flattening. *ACM Trans. Graph.*, 24(2):311–330, 2005.

[30] R. Spigler and M. Vianello. Convergence analysis of the semi-implicit Euler method for abstract evolution equations. *Numer. Funct. Anal. Optim.*, 16:785–803, 1995. MR1341112

[31] O. Trnka, M. Hartman, and K. Svoboda. An alternative semi-implicit Euler method for the integration of highly stiff nonlinear differential equations. *Comput. Chem. Eng.*, 21:277–282, 1996.

[32] Y. Wang, X. Gu, T. Chan, P. M. Thompson, and S.-T. Yau. Intrinsic brain surface conformal mapping using a variational method. In *SPIE International Symposium on Medical Imaging*, 2004.

[33] M.-Q. Wei, M.-Y. Pang, and C.-L. Fan. Survey on planar parameterization of triangular meshes. In *International Conference on Measuring Technology and Mechatronics Automation*, 2010.

[34] Y. Xiao, M. Song, and M. Liu. Convergence and stability of the semi-implicit Euler method with variable stepsize for a linear stochastic pantograph differential equation. *Int. J. Numer. Anal. Model.*, 8:214–225, 2011. MR2740489

Wei-Qiang Huang
Department of Applied Mathematics
National Chiao Tung University
Hsinchu 300
Taiwan
E-mail address: wqhuang@math.nctu.edu.tw

Xianfeng David Gu
Department of Computer Science
Stony Brook University
Stony Brook, NY 11794
USA
E-mail address: gu@cs.sunysb.edu

Tsung-Ming Huang
Department of Mathematics
National Taiwan Normal University
Taipei 116
Taiwan
E-mail address: min@ntnu.edu.tw

Song-Sun Lin
Department of Applied Mathematics
National Chiao Tung University
Hsinchu 300
Taiwan
E-mail address: sslin@math.nctu.edu.tw

Wen-Wei Lin
Department of Applied Mathematics
National Chiao Tung University
Hsinchu 300
Taiwan
E-mail address: wwlin@math.nctu.edu.tw

Shing-Tung Yau
Mathematics Department
Harvard University
Cambridge, MA 02138
USA
E-mail address: yau@math.harvard.edu

Received July 1, 2013